Vesicular Neurotransmitters Exocytosis Monitored by Amperometry: Theoretical Quantitative Links Between Experimental Current Spikes Shapes and Intravesicular Structures.

Supporting Information

Reina Dannaoui,[1] Ren Hu,[2] Lihui Hu,[1] Zhong-Qun Tian,[2] Irina Svir,[1] Wei-Hua Huang,[3] Christian Amatore,[1,2,*] Alexander Oleinick.[1,*]

[1] PASTEUR, Département de Chimie, Ecole normale supérieure, PSL Université, Sorbonne Université, CNRS, 24 rue Lhomond, Paris 75005, France

[2] State Key Laboratory of Physical Chemistry of Solid Surfaces, College of Chemistry and Chemical Engineering, Xiamen University, Xiamen 361005, P.R. China

[3] College of Chemistry and Molecular Sciences, Wuhan University, Wuhan 430072, P.R. China

Content:

A. Extraction procedure of the main parameters shown in Table 1.

The main objectives of this work were: (i) to propose a realistic model accounting for the existence of amperometric spikes displaying one or two exponential decay tails; (ii) to use this model to extract the parameters which govern the shape and intensity of the current of each amperometric spike (see Table 1). Point (i) has been described in detail in the main text, so this section is devoted to describe the principle of the computation procedure developed to answer point (ii).

The script performing the extraction procedure described in the main text and hereafter was implemented in Python 3.8 and ran in Spyder 5.5. The script implementing the extraction procedure developed here and illustrated in section A of Supporting Information is available from the authors on reasonable request.

A.1. Theoretical framework

As follows from our previous work [1] and the discussion in the main text the function $k_{\rho}^{diff}(t)$, is very important in shaping the monitored spikes. For single exponential spikes these functions reach their plateaus rather quickly after the spike peak, a mandatory behavior for the observation of one exponential spikes.[1-3] However, as was discussed in the main text, during the second mode of a two-exponential spike the kinetics of release is essentially governed by $k_1 q_f^0$. This means that the fusion pore size does not contribute directly in sustaining the spike current time variations during this second mode of release. For simplicity it is thus assumed that the pore keeps its maximal size that it achieved at the end of the first exponential mode (see main text). Note that would the pore close during this phase this would lead to a sudden and easily observable decrease of the current as reported in a few instances by Ewing et al.[4]

This allows to formalize the extraction procedure as the optimization problem defined by:

$$\min_{q_0,\, q_f^0, k_1} \Phi \tag{A.1}$$

$$\Phi = \frac{1}{k_\rho^{diff,av2}} \int_{t_{1exp}^{start}}^{t_{2exp}^{fin}} (k_\rho^{diff}(\tau) - k_\rho^{diff,av})^2 d\tau$$

subject to: $$q_0, q_f^0, k_1 > 0, \; q_0 \geq q_f^0$$

where Φ is the objective function indicating deviation of $k_\rho^{diff}(t)$ from its average value $k_\rho^{diff,av}$ during the time range of the first and second exponential regimes:

$$k_\rho^{diff,av} = \frac{1}{t_{2exp}^{fin} - t_{1exp}^{st}} \int_{t_{1exp}^{start}}^{t_{2exp}^{fin}} k_\rho^{diff}(\tau) d\tau$$

where t_{1exp}^{start} and t_{2exp}^{fin} are the times reflecting beginning of the first and end of the second exponential regimes, correspondingly. It should be noted that we found the average value $k_\rho^{diff,av}$ worked well for most of the cases. However, for some noisy spikes an average value was too sensitive to some too large or too small values imposed by noise. In that cases (and in general) using a median value instead of average one provided very good results since it is more robust with respect to outliers.

A.2. Numerical details of the procedure

A.2.1. Algorithm

The Nelder-Mead method was used to solve the optimization problem given above. In order to start optimization procedure, one has to supply initial approximations of the unknown parameters as detailed in the left branch in algorithm shown in Fig.A1.

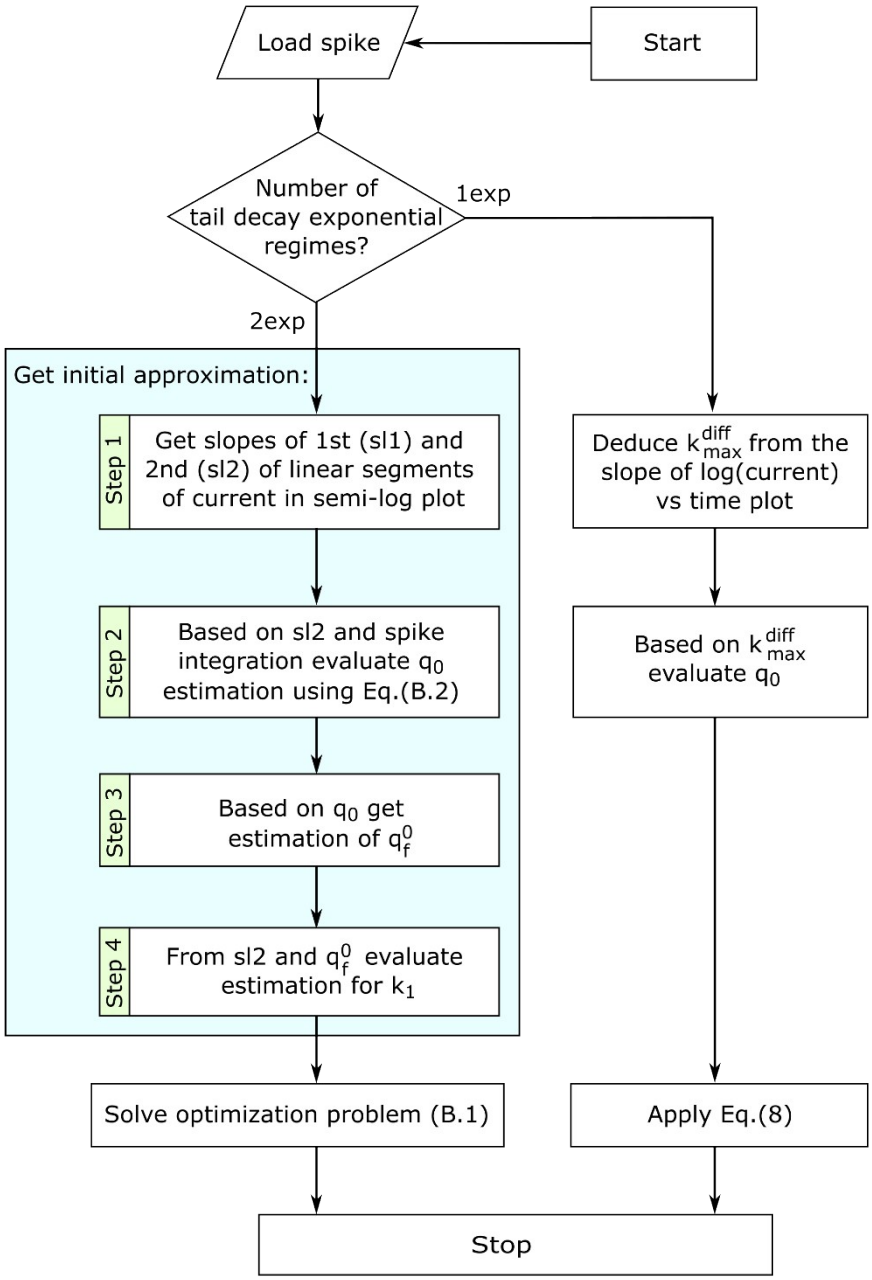

Fig.A1. Algorithm for parameter evaluation required for quantitative treatment of one- and two-exponential spikes with procedures developed here and in previous work.[1]

A.2.2. Description of the steps in the algorithm in Fig.A1 for the two-exponential problem

Step 1. The ranges of the first and second exponential regimes were automatically identified. For this the derivative of the spike was obtained and the width of the minimum well at the level of 75% of its amplitude $[t_{1exp}^{st}, t_{1exp}^{fin}]$ was selected as a duration of the first exponential regime (see Fig.A2). The slope sl_1 was then evaluated from the linear regression of the spike in this range. In principle, the boundaries of the second exponential range can be defined from the signal derivative. However, practically this part is generally saturated with a noise which is amplified even more by differentiation. Thus, we used an alternative approach by performing continuation of the first exponent and noting where it drops to negligible level (ca. 1% of the spike peak) allows to obtain beginning of the second exponential regime, t_{2exp}^{st} (Fig.A2a,b). A t_{2exp}^{fin} value was then defined as

$$t_{2exp}^{fin} = t_{2exp}^{st} + 0.8 \cdot (t_{spike} - t_{2exp}^{st})$$

where t_{spike} is the duration of the spike, in order to reduce the influence of the noise generally encountered at the very end of the signal. The sl_2 value was then computed from a linear regression of the spike at the $[t_{2exp}^{st}, t_{2exp}^{fin}]$ range.

Where necessary, the automatically identified ranges were manually adjusted.

Step 2. Knowing sl_2 value Q_0 was evaluated by using exponential continuation of the spike as it was done for single exponential spikes, but now applied to a second exponential regime.

$$Q_0 = \int_0^{\infty} i(t)dt = \int_0^{t_{spike}} i(t)dt + \int_{t_{spike}}^{\infty} i(t)dt =$$

$$= \int_0^{t_{spike}} i(t)dt + \frac{1}{sl_2} \cdot e^{-sl_2 t_{spike} + b_2} = nFq_0 \qquad \text{(A.2)}$$

where $(-sl_2\, t_{spike} + b_2)$ is the equation of the linear fit of second exponential segment in semi-log plot. Thus, initial approximation for q_0 is obtained.

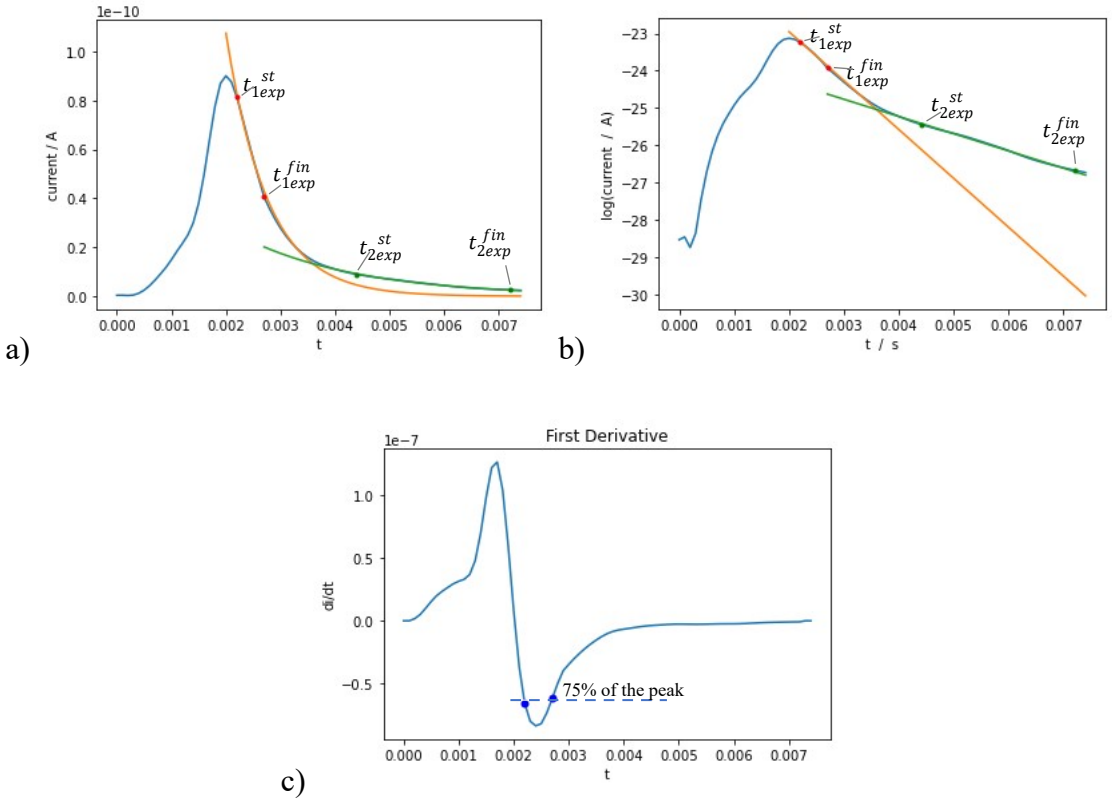

Fig.A2. Automatic determination of the first and second exponential regimes ranges. (a) Current spike; (b) current spike in a semi-log scale; (c) the first derivative of the current.

Step 3. Initial approximation for q_f^0 can then be set based on q_0 value, e.g. $q_f^0 = a \times q_0$, where $a < 1$ and whose value may depend on a dataset to be analyzed.

Step 4. As discussed in the main text the asymptotic value for the slope during second exponential regime in a semi-log plot is $sl_2 = k_1 q_f^0$, hence, initial value of the parameter k_1 was set as $k_1 = - sl_2 / q_f^0$.

For making the extraction procedure more robust with respect to experimental noise inevitably present in the analyzed signal, we used in step 3 a set of initial approximations for q_f^0 (and hence of k_1 in step 4 which is evaluated from q_f^0) in the range $0.4q_0 - 0.85q_0$ with the step of $0.05q_0$. Optimization procedure was repeated for each of the set of initial approximations and the outcome with the smallest Φ value was then selected.

It worth to note that the last term in Eq.(12b), i.e. $k_\rho^{diff}(t)\, q_f$, is the flux of the neurotransmitter flowing through the vesicle pore (see definition in Eq.(12c)). Hence for the reconstruction procedure one may substitute experimental current directly into Eq.(12b) removing the necessity of providing unknown function $k_\rho^{diff}(t)$.

A.2.3. Schematics representation of the procedures for analysis of one- and two-exponential spikes

The essence of the one- and two-exponential spike procedures corresponding to the algorithm are shown below in Figs.A3 and A4.

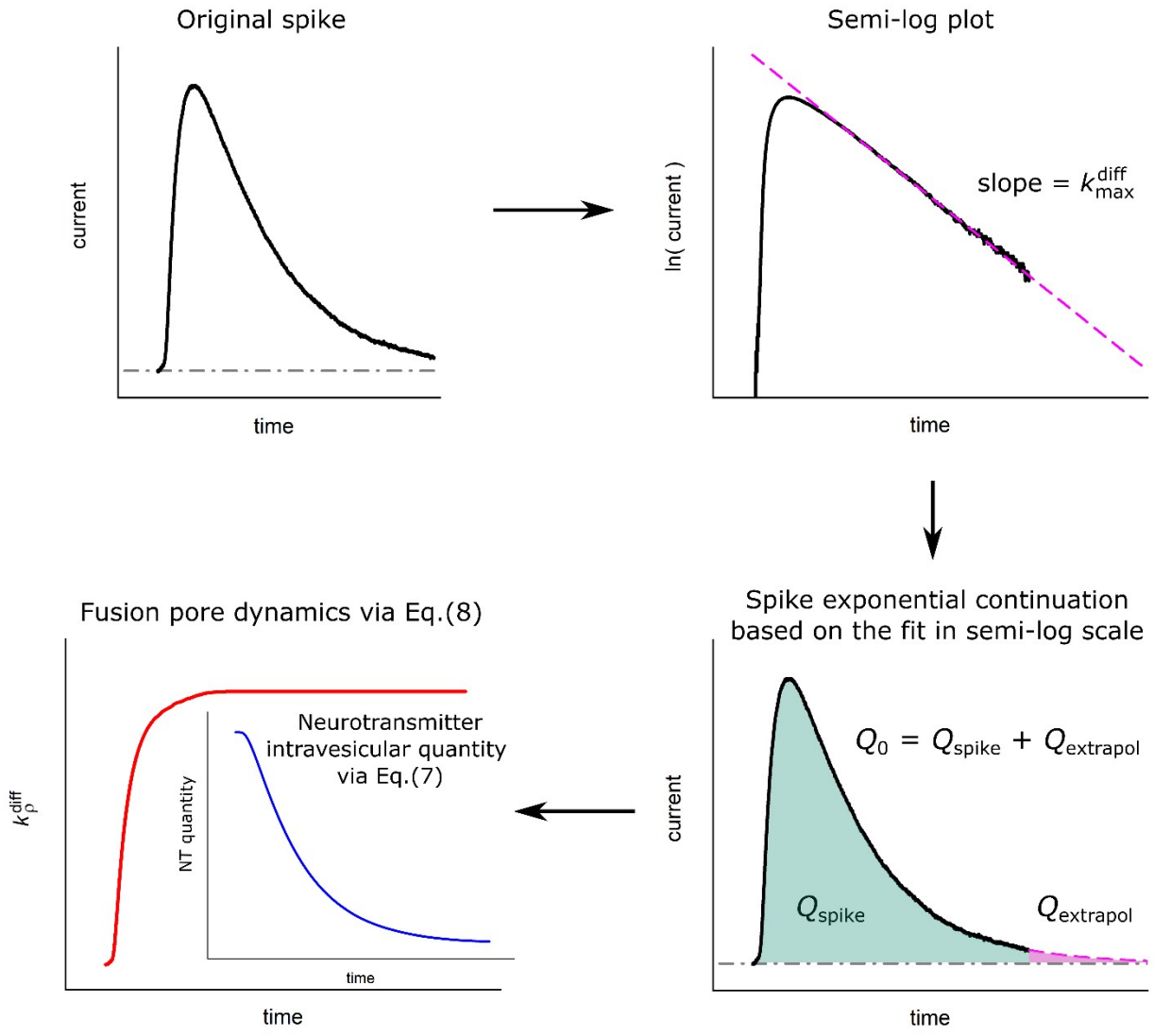

Fig.A3. Schematic depiction of the procedure used to analyze the spikes with one-exponential decay tail.

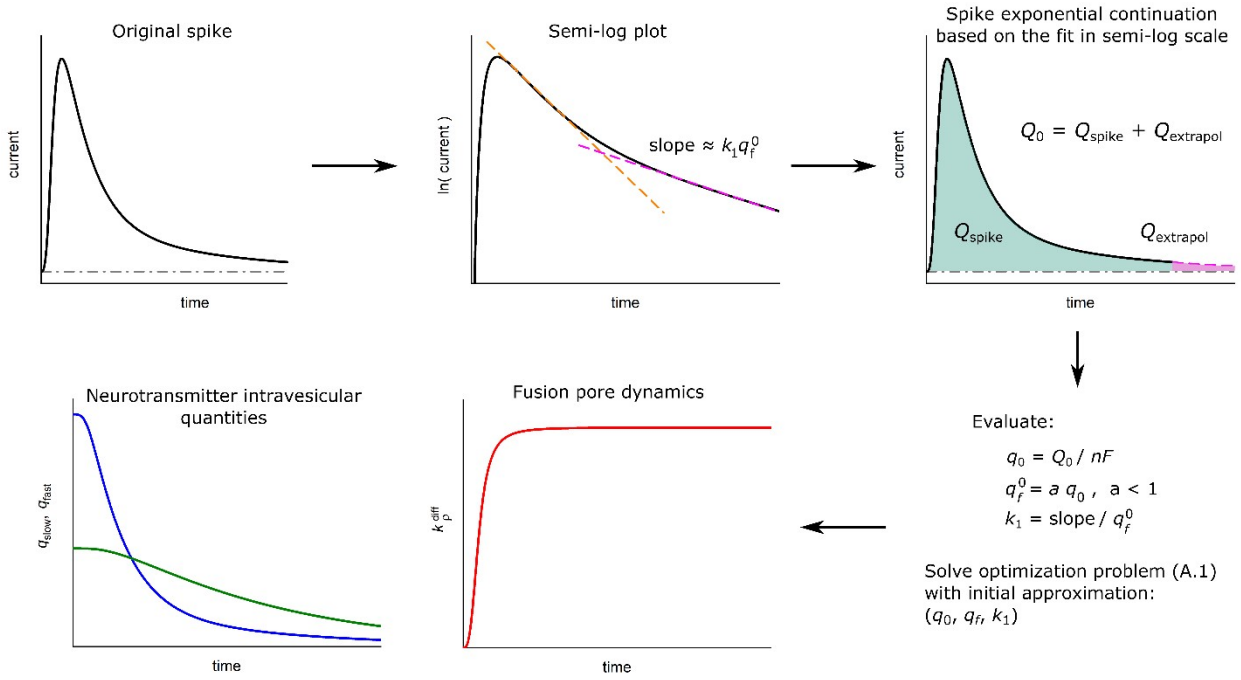

Fig.A4. Schematic depiction of the procedure used to analyze the spikes with two-exponential decay tail.

B. Distribution of k_1 values

The volumes of the highly compacted domains are imposed by local competition between free energy and entropic factors,[5] so they should not vary drastically since the ionic composition of the intravesicular loaded matrices is assumed to be roughly constant. Evaluating analytically their mean volume, $V_{compact}$, hence their number, $N_{compact}$, as may be performed in the conceptually analogous problem of the Debye sphere for colloidal dispersions seems almost impossible except by ad-hoc extended molecular level approaches [6] because of the length and conformation of the chromogranins and the involvement of ionic and non-ionic interactions such as hydrogen bonds. Nonetheless, as a first approximation $V_{compact}$ can be considered as a constant.

On the other hand, for each of these domains the rate constant of interfacial exchange with the surrounding less compacted compartment has to scale with the domains surface, viz., be proportional to $V_{compact}^{2/3}$. Therefore, k_1 as defined in the main text in Eq.(11a) has to be proportional to $N_{compact} \times V_{compact}^{2/3}$, so within this framework one expects that the distribution of k_1 values represents that of $N_{compact}$.

C. General case of reversible exchange between intravesicular domains

As discussed in the text the exchange between the two compartments in general is reversible and prior to the onset of the release (i.e. formation of an initial fusion pore) the exchange between two compartments is necessarily in dynamic equilibrium, but is progressively displaced while the less compacted compartment NT content is released. Hence the exchange between the two phases and extracellular environment in Eqs.(11a,b) is thus replaced by the following kinetic scheme

$$q_s + \emptyset_f \underset{k_2}{\overset{k_1}{\rightleftarrows}} \emptyset_s + q_f \tag{C.1a}$$

$$q_f \overset{k_\rho^{diff}}{\rightarrow} q_{out} \tag{C.1b}$$

where all notations keep their meaning as in the main text and k_2 is the rate constant characterizing reverse exchange from fast to slow compartments. Note that since the interactions between the NT cations and the polyelectrolyte are much stronger in the slow compartment than in the fast one, k_1 features an up-hill reaction while k_2 features down-hill step of the same reaction, hence $k_1 \ll k_2$. In addition, before release one has necessarily $\emptyset_f^0/\emptyset_s^0 = (k_2/k_1) \times (q_f^0/q_s^0)$ in mature vesicles, so the

relatively small amounts of empty sites in the fast and slow compartments are thermodynamically linked to that of NT quantities in each domain.

Within the same framework and assumptions the governing system of differential equations will take the following view:

$$\frac{dq_s}{dt} = -k_1\left(q_f^0 - q_f\right)q_s + k_2\left(q_s^0 - q_s\right)q_f \tag{C.2}$$

$$\frac{dq_f}{dt} = k_1\left(q_f^0 - q_f\right)q_s - k_2\left(q_s^0 - q_s\right)q_f - k_\rho^{diff}(t)q_f \tag{C.3}$$

$$\frac{dq_{out}}{dt} = \frac{i(t)}{nF} = -\left(\frac{dq_s}{dt} + \frac{dq_f}{dt}\right) = k_\rho^{diff}(t)q_f \tag{C.4}$$

associated to the same initial conditions:

$$q^{t=0}_{\ s} = q_s^0, \quad q^{t=0}_{\ f} = q_f^0, \quad q^{t=0}_{\ out} = 0 \tag{C.5}$$

Similarly, to the case considered in the main text the system (C.2, C.3) has two limits depending on the time. At short times, $-\frac{dq_f}{dt} \gg -\frac{dq_s}{dt} \approx 0$ and $q_s \approx q_s^0$ and $dq_s/dt \approx 0$ thus, the same limit is attained as in Eq.(13a) in the main text:

$$\frac{dq_{out}}{dt} = -\frac{dq_f}{dt} \approx k_\rho^{diff}(t)q_f \tag{C.6}$$

and the same time constant $\tau_1 = 1/k_{max}^{diff}$ controls the release during first exponential regime.

Conversely, when the fast compartment is almost emptied, viz. when $q_f \ll q_f^0$ and $q_s^0 \gg q_s$, release is essentially commanded kinetically by the transfer of NT molecules from the slow compartment into the fast one in which they rapidly exit the vesicle through the fusion pore. In other words, NT

quantity in the fast compartment is under steady state, so that:

$$q_f \longrightarrow \frac{k_1 q_f^0}{[k_2 q_s^0 + k_\rho^{diff}(t)]} q_s \tag{C.7}$$

Hence the current at long times:

$$\frac{i(t)}{nF} = \frac{dq_{out}}{dt} \approx - \frac{dq_s}{dt} \approx \frac{k_1 q_f^0 k_\rho^{diff}(t)}{[k_2 q_s^0 + k_\rho^{diff}(t)]} q_s \tag{C.8}$$

controlled by the following time constant $\tau_2 = [k_2 q_s^0 + k_{max}^{diff}]/(k_1 q_f^0 k_{max}^{diff})$. Equation (C.7), hence also Eq. (C.8), admits two limits depending on the relative magnitude of $k_2 q_s^0$ vs. $k_\rho^{diff}(t)$. Would $k_2 q_s^0$ be much larger than $k_\rho^{diff}(t)$, the initial equilibrium between the slow and fast compartments would always be maintained during release so that:

$$\frac{dq_{out}}{dt} \approx \frac{k_1 q_f^0}{k_2 q_s^0} k_\rho^{diff}(t) q_s \tag{C.9}$$

However, the latter does not seem to be the case. Indeed, although polyelectrolyte/neurotransmitter condensed state is thermodynamically favorable (as discussed above), this step necessarily requires numerous local molecular rearrangements (e.g. change in polyelectrolyte conformation, expel of the solvent molecules during polyelectrolyte condensation etc.) which might determine the kinetics of the exchange process making diffusion controlled release a prevailing process. Under these conditions the opposite limiting case likely takes place, i.e. when $k_\rho^{diff}(t) \gg k_2 q_s^0$ and again the limit identical to the one in Eq.(8c) is attained:

$$\frac{dq_{out}}{dt} \approx - \frac{dq_s}{dt} \approx k_1 q_f^0 q_s \tag{C.10}$$

with a time constant $\tau_2 = 1/(k_1 q_f^0)$ controlling the release.

References:

[1] A. Oleinick, I. Svir, C. Amatore, 'Full fusion' is not ineluctable during vesicular exocytosis of neurotransmitters by endocrine cells, Proc. Roy. Soc. A. 473 (2017) 20160684.

[2] C. Amatore, A.I. Oleinick, I. Svir, Diffusion from within a Spherical Body with Partially Blocked Surface: Diffusion through a Constant Surface Area, ChemPhysChem. 11 (2010) 149–158.

[3] C. Amatore, A.I. Oleinick, I. Svir, Reconstruction of Aperture Functions during Full Fusion in Vesicular Exocytosis of Neurotransmitters, ChemPhysChem. 11 (2010) 159–174.

[4] L.J. Mellander, R. Trouillon, M.I. Svensson, A.G. Ewing, Amperometric post spike feet reveal most exocytosis is via extended kiss-and-run fusion, Sci Rep. 2 (2012) 907.

[5] M. Muthukumar, Theory of counter-ion condensation on flexible polyelectrolytes: Adsorption mechanism, The Journal of Chemical Physics 120 (2004) 9343–9350.

[6] see <https://www.ebi.ac.uk/pdbe/entry/pdb/1n2y> and the molecular dynamics snapshots presented therein.